ARTICLE

New Hexagonal-rhombic Trilayer Ice Structure Confined between Hydrophobic Plates

Min Jia, Wen-hui Zhao, Lan-feng Yuan*

Hefei National Laboratory for Physical Sciences at the Microscale, University of Science and Technology of China, Hefei 230026, China

(Dated: Received on May 22, 2013; Accepted on May 29, 2013)

We perform molecular dynamics simulations for water confined between two smooth hydrophobic walls and observe two crystalline structures with one being first reported. Both of these structures obey the ice rule. The novel ice phase is a flat hexagonal-rhombic trilayer ice, obtained under 1 GPa load at wall separation of 1.0 nm. In this structure, the water molecules in the two layers next to one of the walls (outer layers) and in the middle layer form hexagonal rings and rhombic rings, respectively. For a molecule in the outer layers, three of its four hydrogen bonds are in the same layer, and the other one hydrogen bond connects to the middle layer. For a molecule in the middle layer, only two of its four hydrogen-bonds are located in the same layer, and the other two connect to two different outer layers. Despite their different motifs, the area densities of the three layers are almost equal. The other structure is a flat hexagonal bilayer ice produced at wall separation of 0.8 nm under lateral pressure of 100 MPa, analogous to a system demonstrated by Koga *et al.* [Phys. Rev. Lett. **79**, 5262 (1997)]. Both first-order and continuous phase transitions take place in these simulations.

Key words: Confined water, Molecular dynamics, Hexagonal-rhombic trilayer ice, Hexagonal-rhombic trilayer ice

I. INTRODUCTION

Confinement disrupts the hydrogen bonding network in bulk water, leading to novel and intriguing structures and properties of confined water different from their bulk counterparts. Because of the important role of confined water in biology, geophysics and advanced technology, in recent years this area has attracted a great deal of interests [1−10].

On one-dimensional structures, Zangi and collaborators studied the freezing of water in carbon nanotubes or under confinement by atomically detailed walls with dispersive, nondirectional interactions, showing the importance of substrate geometry on freezing [11, 12]. On two-dimensional structures, Han *et al.* demonstrated that in a hydrophobic nanoslit, the freezing of bilayer water may occur continuously as well as discontinuously through a first-order phase transition [13]. A first-order water-to-ice freezing transition and a bilayer hexagonal ice phase were observed by Koga *et al.* via cooling along with compression of bilayer water in a nanopore with smooth walls [14, 15]. For water between walls with separation of 1.1 nm, Kumar *et al.* observed that a trilayer liquid transforms into a bilayer liquid with decrease of its density [16].

There are also some trilayer ices possessing long-range order in the configuration of oxygen atoms. With increases of the confined water density, Giovambattista *et al.* found a first-order transition from bilayer liquid to trilayer heterogeneous fluid (THF) which was characterized by a liquid (central) layer and two crystal-like layers next to the walls [17]. As Zangi *et al.* observed in their simulations, confined water at temperature of T=280 K can be induced to crystallize under the influence of external lateral electric field with magnitude of 5 V/nm [18]. They found two crystals: a low-density ice built from hexagonal rings parallel to the confining walls and a high-density ice built from rhombic rings.

In the present work, we investigate the freezing transitions and structures of water confined between two hydrophobic parallel walls via molecular dynamics simulations. Two crystalline structures are observed, and one of them has not been reported in literature. This new ice phase is a flat hexagonal-rhombic trilayer ice (fHRTI), obtained under 1 GPa load at wall separation d=1.0 nm. The other crystalline phase is a flat hexagonal bilayer ice (fHBI) produced from the simulation at d=0.8 nm and lateral pressure P_{L}=100 MPa, and it is analogous to a system reported by Koga *et al.* [14].

*Author to whom correspondence should be addressed. E-mail: yuanlf@ustc.edu.cn

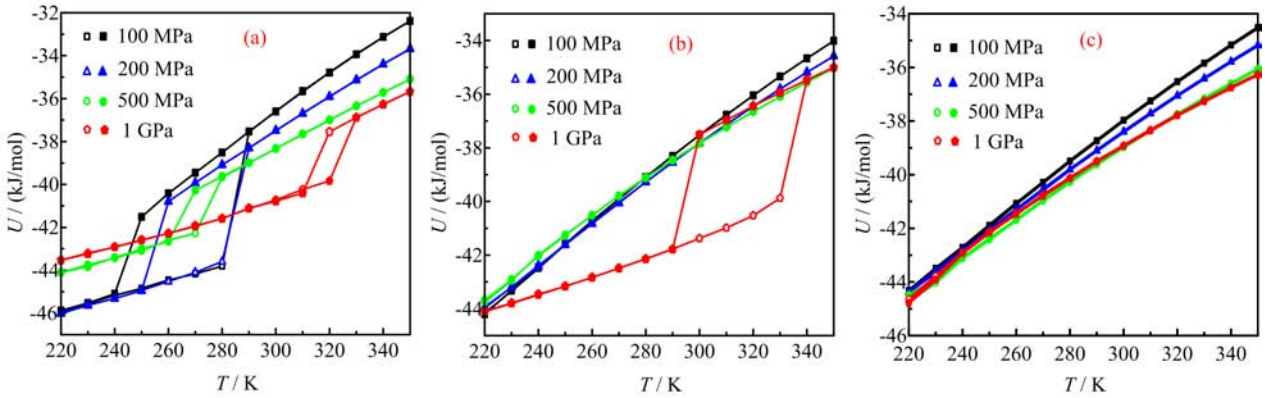

FIG. 1 Potential energy U as a function of T for various lateral pressure at different wall separations. (a) d=0.8 nm, (b) d=1.0 nm, (c) d=1.2 nm. The cooling process and heating process are indicated by the solid and open symbols, respectively.

II. METHODS

We use the GROMACS simulation package [19] to simulate a system of 400 water molecules confined between two infinite smooth hydrophobic parallel walls. The five-site tetrahedrally coordinated model of TIP5P [20] is used to describe the water molecules. The wall-wall separation d is set to be in the range from 0.8 nm to 1.2 nm, with an increment of 0.2 nm. The direction perpendicular to the walls is chosen as z, and the middle slab with equal distances to the two walls is defined as z=0. Periodic boundary conditions are imposed in the x and y directions, parallel to the walls. The water-wall interactions are modeled by a 9-3 Lennard-Jones potential which is commonly used to represent the effective interactions of water molecules with the confining surfaces. This potential function is shown as follows [21−25]:

$$U(\Delta z) = 4\varepsilon_{\text{o-wl}}\left[\left(\frac{\sigma_{\text{o-wl}}}{\Delta z}\right)^9 - \left(\frac{\sigma_{\text{o-wl}}}{\Delta z}\right)^3\right] \qquad (1)$$

here Δz is the distance from the oxygen atom of a water molecule to the wall, whereas $\sigma_{\text{o-wl}}$=0.25 nm and $\varepsilon_{\text{o-wl}}$=1.25 kJ/mol are potential parameters, this set of parameter values were commonly used in simulations for confined water [26−28]. The ensemble is with constant number of molecules, P_{L} and T. The Nosé-Hoover thermostat [29, 30] and Parrinello-Rahman barostat [31] are employed to control the temperature and pressure. Due to the non-periodicity in z direction, the long-range electrostatic interactions are treated with the slab-adapted Ewald sum method [32], and a cutoff of 1 nm is used for van der Waals and Coulomb interactions in real space. The simulation for each set of T and d is carried out for 50 ns with a step of 2 fs.

III. RESULTS

The MD simulations for various d and P_{L} are performed. For each P_{L}, the T is first lowered from 350 K to 160 K with a step of 10 K and then raised in the same way. As Fig.1(a) shows, in the MD simulations for d=0.8 nm, the potential energy U first gradually decreases with cooling of the system, and then suddenly drops by about 3−5 kJ/mol to a lower value. Analogously, upon heating the potential energy jumps to a higher value, but at a temperature higher than the transition temperature in the cooling process. In addition to the MD simulation for d=0.8 nm, the potential energies of system under 1 GPa load at d=1.0 nm also exhibit these abrupt changes. These phase transitions are identified as first-order. Moreover, these first-order transitions between liquid and solid are accompanied by discontinuities of 3−4 orders of magnitude in the lateral diffusion coefficient D_{L}, as shown in Fig.2. For example, in the cooling process at d=0.8 nm and P_{L}=100 MPa and T=250 K, $D_{\text{L}}\approx 2.0\times10^{-6}$ cm^2/s; for the same system at 240 K , $D_{\text{L}}\approx 1.2\times10^{-11}$ cm^2/s. In the other simulations, those are no sharp changes in the U and D_{L}, while the D_{L} gradually decrease under 10^{-8} cm^2/s, so we attribute them to continuous phase transitions. The lines of potential energy in the cooling and heating processes for continuous phase transitions are almost in registry.

With cooling of the system, confined liquid water transforms into ice phases, including ten amorphous structures and two crystal-like structures in which one has not be reported in literature. We now turn attention to these structures. Based on the snapshots, their inherent configurations are obtained as the potential-energy local minimum structure by applying steepest-descent method. The inherent structures of the two crystalline phases and a representative amorphous structure are shown in Figs. 3, 4, and 5, respecvtively.

Figure 3 shows the top and side views of a flat hexagonal bilayer ice (fHBI) obtained at d=0.8 nm and

DOI:10.1063/1674-0068/27/01/15-19

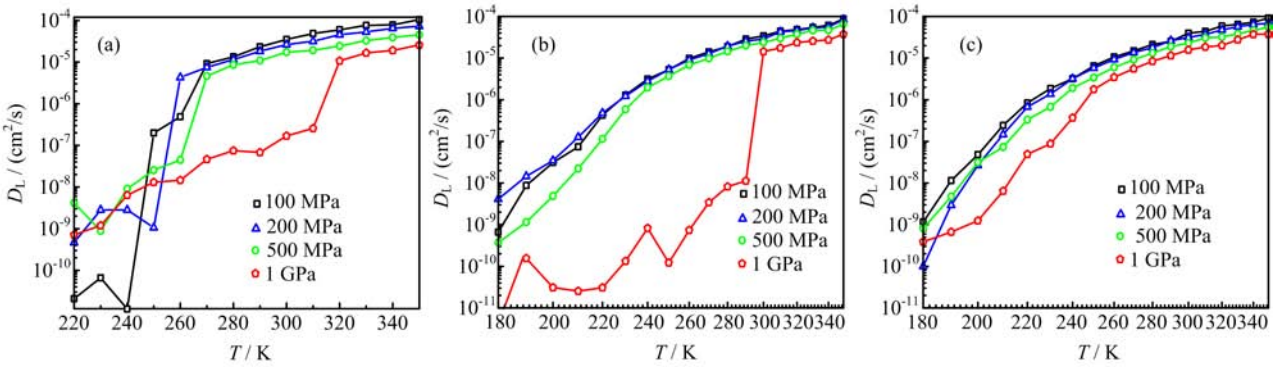

FIG. 2 The lateral diffusion coefficient D_L as a function of temperature T for various lateral pressure in the cooling process at different wall separations. (a) d=0.8 nm, (b) d=1.0 nm, (c) d=1.2 nm.

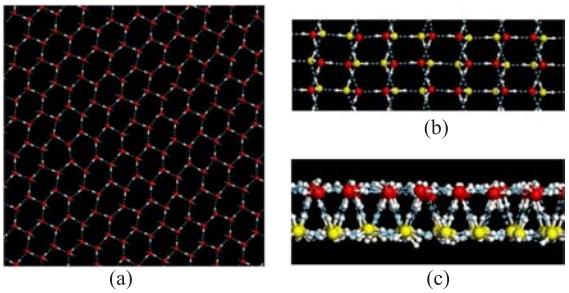

FIG. 3 Inherent configuration of fHBI obtained from MD simulation at P_L=100 MPa, T=240 K and d=0.8 nm. (a) Top view of the upper layer of this hexagonal bilayer lattice structure. (b) Zoomed top view of fHBI. (c) Side view of fHBI. Oxygen atoms in upper and lower layer are depicted in red and yellow, respectively; and hydrogen bonds in blue dotted lines.

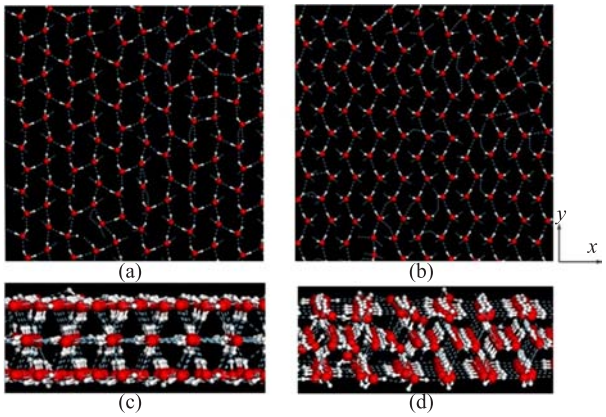

FIG. 4 Inherent structure of fHRTI obtained from MD simulation at d=1.0 nm and P_L=1 GPa. (a, b) Top view of the ice layer next to one of the walls and at the middle slab. (c, d) Side view of fHRTI at direction of x and y. Oxygen atoms are depicted in red, hydrogen atoms in white, and hydrogen bonds in blue dotted lines.

P_L=100 MPa and T=240 K. The water molecules in both layers form hexagonal rings, and all the oxygen atoms in each layer are located in the same plane. As a measure of the planarity of a layer, the width of the transverse density profile (TDP) of oxygen atoms is less than 0.05 nm (as shown in Fig.6(a)). This structure obeys the ice rule, *i.e.*, every molecule participates in four hydrogen bonds. Among these four hydrogen bonds, three are in the same layer, and the fourth one connects to a molecule in the opposite layer. As shown in Fig.7, the hydrogen bond O−H$\cdots$O angle distribution exhibits a peak around 167° and a shoulder ranging from 140° to 160°. The small angles of the shoulder are originated from the hydrogen bonds in the same planes. An analogous structure was reported by Koga *et al.* [13], which was also a flat hexagonal bilayer ice. Nevertheless, there are still some differences between these two structures. In their simulations, the upper and lower distorted hexagonal lattices were completely in registry. While in this work, the oxygen atoms in the two layers are regularly staggered, as displayed in Fig.3(b).

We obtain another polymorph of ice under 1 GPa load at wall separation d=1.0 nm, which is previously unknown. Its TDP exhibits three peaks, as Fig.6(b) shows. At high temperature, the peak height of the central peak is lower than those of the other two peaks. When the temperature decreases from 300 K to 290 K, the heights of all the three peaks jump to higher values that are nearly equal. Meanwhile, the lateral diffusion coefficient D_L drops from 1.45×10^{-5} cm^2/s to 1.13×10^{-8} cm^2/s (Fig.2(b)) and the potential energy shows a sharp change of about 4 kJ/mol (Fig.1(b)), indicating a first-order transition between liquid and solid. In this ice phase (Fig.4 (a)−(d)), the oxygen atoms form three flat planes; the water molecules in the two layers next to one of the walls (outer layers) and in the middle layer form hexagonal and rhombic rings, respectively. So we name this structure as fHRTI. In the middle layer, a minimum repeating unit consists of two rhmobuses with different directions. Despite the different motifs in the outer layers and in the middle layer, the area densities of the three layers are nearly equal:

DOI:10.1063/1674-0068/27/01/15-19

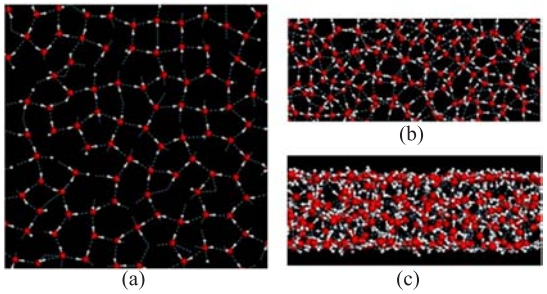

FIG. 5 Inherent structure obtained from MD simulation at d=1.2 nm and P_{L}=1 GPa. (a) The top view of the upper layer of this amorphous structure. (b) The zoomed top view of the amorphous. (c) The side view of the amorphous. Oxygen atoms are depicted in red, hydrogen atoms in white, and hydrogen bonds in blue dotted lines.

the numbers of oxygen atoms in the three layers (up to down) are 132, 136, and 132, respectively. This is also reflected in the three TDP peaks with similar heights and widths (Fig.6(b)).

As the case of fHBI, each water molecule in fHRTI also possesses four hydrogen bonds. For a molecule in the outer layers, three of its hydrogen bonds are in the same layer, and the other one connects to a molecule in the middle layer. On the other hand, for a molecule in the middle layer, two hydrogen bonds are in the same layer, and the other two connect to the two different outer layers. The distribution of O−H$\cdots$O angles of hydrogen bonds (Fig.7) exhibits a peak around 162° and a shoulder around 118°, *i.e.*, some hydrogen bonds are heavily bent. These bent hydrogen bonds are between neighboring molecules of the outer layers in the chains in y direction (Fig.4(a)).

Among the ten amorphous structures, we pick the one at P_{L}=1 GPa and d=1.2 nm as an example, and show its inherent structure in Fig.5. Its TDP exhibits four peaks (or two peaks and two shoulders), and shows no sharp change with change of temperature (Fig.6(c)). The densities of layers near the wall are significantly higher than the middle two layers. Therefore, the composition of this structure may be called either four layers or two puckered layers. This amorphous structure lacks long-range order in the configuration of oxygen atoms, resulting in diverse and complicated hydrogen bonding patterns.

IV. CONCLUSION

In this work we have employed extensive MD simulations of water confined between two hydrophobic parallel walls for three separations: d=0.8, 1.0, 1.2 nm. Both first-order and continuous phase transitions are observed.

Two kinds of crystalline ice phase fHBI and fHRTI are formed spontaneously, and fHRTI is first ever reported.

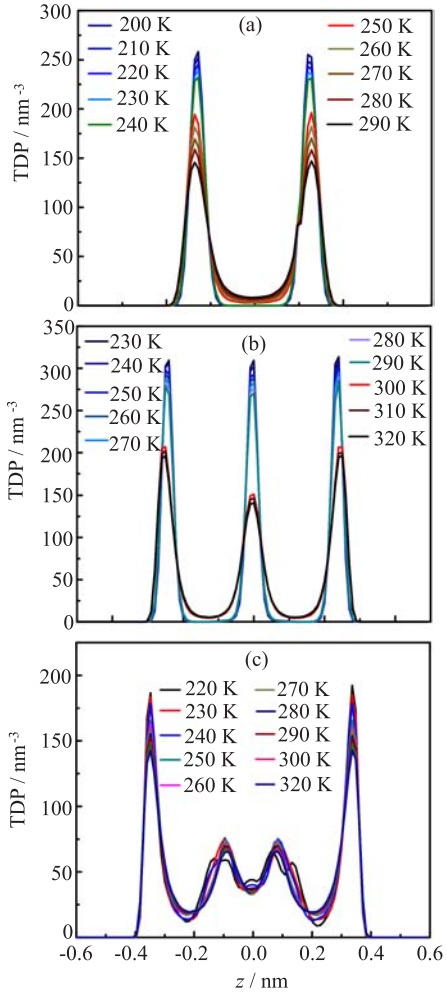

FIG. 6 The TDP of oxygen atoms at different d, P_{L}, and T. The TDP depending on T at (a) d=0.8 nm, (b) d=1.0 nm, and (c) d=1.2 nm.

In both structures, each water molecule has four hydrogen bonds. The fHRTI is composed of two outer layers of hexagonal rings and a middle layer of rhombic rings. Among the four hydrogen bonds of a molecule in the outer layers, three are in the same layer, and the other one connects to the middle layer. For a molecule in the middle layer, only two hydrogen bonds are in the same layer, and the other two connect to the two different outer layers. These novel and interesting findings on bilayer and trilayer ices deepen our understanding for confined water.

V. ACKNOWLEDGMENTS

This work was supported by the National Natural Science Foundation of China (No.20603032, No.20733004, No.21121003, No.91021004, and No.20933006), by the Ministry of Science and Technology of China (No.2011CB921400), the National Excellent Doc-

DOI:10.1063/1674-0068/27/01/15-19

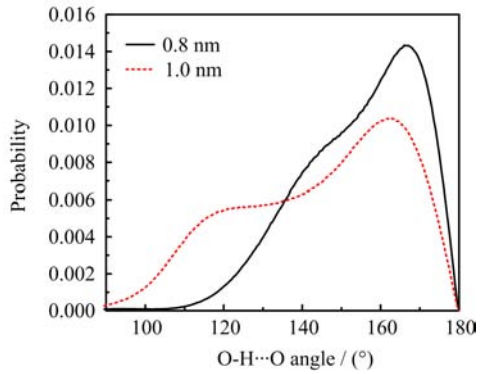

FIG. 7 Distribution of hydrogen bond angles for fHBI (solid line) and fHRTI (dotted line).

toralDissertation of China (No.200736), the Fundamental Research Funds for the Central Universities (No.WK2340000006, No.WK2060140005, and No.WK2060030012), and the USTC-HP HPC Project.

[1] K. Koga, H. Tanaka, and X. C. Zeng, Nature **408**, 564 (2000).
[2] K. Koga, G. T. Gao, H. Tanaka, and X. C. Zeng, Nature **412**, 802 (2001).
[3] R. J. Mashl, S. Joseph, N. R. Aluru, and E. Jakobsson, Nano Lett. **3**, 589 (2003).
[4] J. Bai, C. R. Su, R. D. Parra, X. C. Zeng, H. Tanaka, K. Koga, and J. M. Li, J. Chem. Phys. **118**, 3913 (2003).
[5] Y. Liu, Q. Wang, T. Wu, and L. Zhang, J. Chem. Phys. **123**, 234701-1 (2005).
[6] D. Takaiwa, I. Hatano, K. Koga, and H. Tanaka, Proc. Natl. Acad. Sci. USA **105**, 39 (2008).
[7] N. Kastelowitz, J. C. Johnston, and V. Molinero, J. Chem. Phys. **132**, 124511 (2010).
[8] K. Xu, P. Cao, and J. R. Heath, Science **329**, 1188 (2010).
[9] R. M. Kumar, M. Elango, R. Parthasarathi, and V. Subramanian, J. Phys. Chem. A **115**, 12841 (2011).
[10] C. Guse and R. Hentschke, J. Phys. Chem. B **116**, 751 (2012).
[11] J. Bai, J. Wang, and X. C. Zeng, Proc. Natl. Acad. Sci. USA **103**, 19664 (2006).
[12] R. Zangi and A. Mark, Phys. Rev. Lett. **91**, 025502 (2003).
[13] S. Han, M. Y. Choi, P. Kumar, and H. E. Stanley, Nat. Phys. **10**, 1038 (2010).
[14] K. Koga, X. C. Zeng, and H. Tanaka, Phys. Rev. Lett. **79**, 5262 (1997).
[15] J. C. Johnston, N. Kastelowitz, and V. Molinero, J. Chem. Phys. **132**, 124511 (2010).
[16] P. Kumar, S. V. Buldyrev, F. W. Starr, N. Giovambattista, and H. E. Stanley, Phys. Rev. E **72**, 051503 (2005).
[17] N. Giovambattista, P. J. Rossky, and P. G. Debenedetti, Phys. Rev. Lett. **102**, 050603-1 (2009).
[18] R. Zangi and A. E. Mark, J. Chem. Phys. **120**, 7123 (2004).
[19] B. Hess, C. Kutzner, D. van der Spoel, and E. Lindahl, J. Chem. Theory Comput. **4**, 435 (2008).
[20] M. W. Mahoney and W. L. Jorgensen, J. Chem. Phys. **112**, 8910 (2000).
[21] S. Han, P. Kumar, and H. E. Stanley, Phys. Rev. E **79**, 041202 (2009).
[22] P. Kumar, S. V. Buldyrev, F. W. Starr, N. Giovambattista, and H. E. Stanley, Phys. Rev. E **72**, 051503-1 (2005).
[23] K. Koga and H. Tanaka, J. Chem. Phys. **122**, 104711-1 (2005).
[24] J. Bai, C. A. Angell, and X. C. Zeng, Proc. Natl. Acad. Sci. USA **107**, 5718 (2010).
[25] D. Bratko, C. D. Daub, and A. Luzar, Phys. Chem. Chem. Phys. **10**, 6807 (2008).
[26] S. H. Han, M. Y. Choi, P. Kumar, and H. E. Stanley, Nat. Phys. **6**, 685 (2010).
[27] C. Y. Lee, J. A. McCammon, and P. J. Rossky, J. Chem. Phys. **80**, 4448 (1984).
[28] S. H. Lee and P. J. Rossky, J. Chem. Phys. **100**, 3334 (1994).
[29] S. Nosé and M. L. Klein, Mol. Phys. **50**, 1055 (1983).
[30] W. G. Hoover, Phys. Rev. **A31**, 1695 (1985).
[31] M. Parrinello and A. Rahman, J. Appl. Phys. **52**, 7182 (1981).
[32] I. C. Yeh and M. L. Berkowitz, J. Chem. Phys. **111**, 3155 (1999).

DOI:10.1063/1674-0068/27/01/15-19